Search for $B \to K^{(*)}\nu\bar{\nu}$ and invisible quarkonium decays

J. P. Lees,[1] V. Poireau,[1] V. Tisserand,[1] E. Grauges,[2] A. Palano,[3a,3b] G. Eigen,[4] B. Stugu,[4] D. N. Brown,[5] L. T. Kerth,[5] Yu. G. Kolomensky,[5] M. Lee,[5] G. Lynch,[5] H. Koch,[6] T. Schroeder,[6] C. Hearty,[7] T. S. Mattison,[7] J. A. McKenna,[7] R. Y. So,[7] A. Khan,[8] V. E. Blinov,[9] A. R. Buzykaev,[9] V. P. Druzhinin,[9] V. B. Golubev,[9] E. A. Kravchenko,[9] A. P. Onuchin,[9] S. I. Serednyakov,[9] Yu. I. Skovpen,[9] E. P. Solodov,[9] K. Yu. Todyshev,[9] A. N. Yushkov,[9] D. Kirkby,[10] A. J. Lankford,[10] M. Mandelkern,[10] B. Dey,[11] J. W. Gary,[11] O. Long,[11] G. M. Vitug,[11] C. Campagnari,[12] M. Franco Sevilla,[12] T. M. Hong,[12] D. Kovalskyi,[12] J. D. Richman,[12] C. A. West,[12] A. M. Eisner,[13] W. S. Lockman,[13] A. J. Martinez,[13] B. A. Schumm,[13] A. Seiden,[13] D. S. Chao,[14] C. H. Cheng,[14] B. Echenard,[14] K. T. Flood,[14] D. G. Hitlin,[14] P. Ongmongkolkul,[14] F. C. Porter,[14] R. Andreassen,[15] Z. Huard,[15] B. T. Meadows,[15] M. D. Sokoloff,[15] L. Sun,[15] P. C. Bloom,[16] W. T. Ford,[16] A. Gaz,[16] U. Nauenberg,[16] J. G. Smith,[16] S. R. Wagner,[16] R. Ayad,[17,*] W. H. Toki,[17] B. Spaan,[18] K. R. Schubert,[19] R. Schwierz,[19] D. Bernard,[20] M. Verderi,[20] S. Playfer,[21] D. Bettoni,[22a] C. Bozzi,[22a] R. Calabrese,[22a,22b] G. Cibinetto,[22a,22b] E. Fioravanti,[22a,22b] I. Garzia,[22a,22b] E. Luppi,[22a,22b] L. Piemontese,[22a] V. Santoro,[22a] R. Baldini-Ferroli,[23] A. Calcaterra,[23] R. de Sangro,[23] G. Finocchiaro,[23] S. Martellotti,[23] P. Patteri,[23] I. M. Peruzzi,[23,†] M. Piccolo,[23] M. Rama,[23] A. Zallo,[23] R. Contri,[24a,24b] E. Guido,[24a,24b] M. Lo Vetere,[24a,24b] M. R. Monge,[24a,24b] S. Passaggio,[24a] C. Patrignani,[24a,24b] E. Robutti,[24a] B. Bhuyan,[25] V. Prasad,[25] M. Morii,[26] A. Adametz,[27] U. Uwer,[27] H. M. Lacker,[28] P. D. Dauncey,[29] U. Mallik,[30] C. Chen,[31] J. Cochran,[31] W. T. Meyer,[31] S. Prell,[31] A. E. Rubin,[31] A. V. Gritsan,[32] N. Arnaud,[33] M. Davier,[33] D. Derkach,[33] G. Grosdidier,[33] F. Le Diberder,[33] A. M. Lutz,[33] B. Malaescu,[33] P. Roudeau,[33] A. Stocchi,[33] G. Wormser,[33] D. J. Lange,[34] D. M. Wright,[34] J. P. Coleman,[35] J. R. Fry,[35] E. Gabathuler,[35] D. E. Hutchcroft,[35] D. J. Payne,[35] C. Touramanis,[35] A. J. Bevan,[36] F. Di Lodovico,[36] R. Sacco,[36] G. Cowan,[37] J. Bougher,[38] D. N. Brown,[38] C. L. Davis,[38] A. G. Denig,[39] M. Fritsch,[39] W. Gradl,[39] K. Griessinger,[39] A. Hafner,[39] E. Prencipe,[39] R. J. Barlow,[40,‡] G. D. Lafferty,[40] E. Behn,[41] R. Cenci,[41] B. Hamilton,[41] A. Jawahery,[41] D. A. Roberts,[41] R. Cowan,[42] D. Dujmic,[42] G. Sciolla,[42] R. Cheaib,[43] P. M. Patel,[43,§] S. H. Robertson,[43] P. Biassoni,[44a,44b] N. Neri,[44a] F. Palombo,[44a,44b] L. Cremaldi,[45] R. Godang,[45,‖] P. Sonnek,[45] D. J. Summers,[45] X. Nguyen,[46] M. Simard,[46] P. Taras,[46] G. De Nardo,[47a,47b] D. Monorchio,[47a,47b] G. Onorato,[47a,47b] C. Sciacca,[47a,47b] M. Martinelli,[48] G. Raven,[48] C. P. Jessop,[49] J. M. LoSecco,[49] K. Honscheid,[50] R. Kass,[50] J. Brau,[51] R. Frey,[51] N. B. Sinev,[51] D. Strom,[51] E. Torrence,[51] E. Feltresi,[52a,52b] M. Margoni,[52a,52b] M. Morandin,[52a] M. Posocco,[52a] M. Rotondo,[52a] G. Simi,[52a] F. Simonetto,[52a,52b] R. Stroili,[52a,52b] S. Akar,[53] E. Ben-Haim,[53] M. Bomben,[53] G. R. Bonneaud,[53] H. Briand,[53] G. Calderini,[53] J. Chauveau,[53] Ph. Leruste,[53] G. Marchiori,[53] J. Ocariz,[53] S. Sitt,[53] M. Biasini,[54a,54b] E. Manoni,[54a] S. Pacetti,[54a,54b] A. Rossi,[54a,54b] C. Angelini,[55a,55b] G. Batignani,[55a,55b] S. Bettarini,[55a,55b] M. Carpinelli,[55a,55b,¶] G. Casarosa,[55a,55b] A. Cervelli,[55a,55b] F. Forti,[55a,55b] M. A. Giorgi,[55a,55b] A. Lusiani,[55a,55c] B. Oberhof,[55a,55b] E. Paoloni,[55a,55b] A. Perez,[55a] G. Rizzo,[55a,55b] J. J. Walsh,[55a] D. Lopes Pegna,[56] J. Olsen,[56] A. J. S. Smith,[56] R. Faccini,[57a,57b] F. Ferrarotto,[57a] F. Ferroni,[57a,57b] M. Gaspero,[57a,57b] L. Li Gioi,[57a] G. Piredda,[57a] C. Bünger,[58] O. Grünberg,[58] T. Hartmann,[58] T. Leddig,[58] C. Voß,[58] R. Waldi,[58] T. Adye,[59] E. O. Olaiya,[59] F. F. Wilson,[59] S. Emery,[60] G. Hamel de Monchenault,[60] G. Vasseur,[60] Ch. Yèche,[60] F. Anulli,[61] D. Aston,[61] D. J. Bard,[61] J. F. Benitez,[61] C. Cartaro,[61] M. R. Convery,[61] J. Dorfan,[61] G. P. Dubois-Felsmann,[61] W. Dunwoodie,[61] M. Ebert,[61] R. C. Field,[61] B. G. Fulsom,[61] A. M. Gabareen,[61] M. T. Graham,[61] C. Hast,[61] W. R. Innes,[61] P. Kim,[61] M. L. Kocian,[61] D. W. G. S. Leith,[61] P. Lewis,[61] D. Lindemann,[61] B. Lindquist,[61] S. Luitz,[61] V. Luth,[61] H. L. Lynch,[61] D. B. MacFarlane,[61] D. R. Muller,[61] H. Neal,[61] S. Nelson,[61] M. Perl,[61] T. Pulliam,[61] B. N. Ratcliff,[61] A. Roodman,[61] A. A. Salnikov,[61] R. H. Schindler,[61] A. Snyder,[61] D. Su,[61] M. K. Sullivan,[61] J. Va'vra,[61] A. P. Wagner,[61] W. F. Wang,[61] W. J. Wisniewski,[61] M. Wittgen,[61] D. H. Wright,[61] H. W. Wulsin,[61] V. Ziegler,[61] W. Park,[62] M. V. Purohit,[62] R. M. White,[62,**] J. R. Wilson,[62] A. Randle-Conde,[63] S. J. Sekula,[63] M. Bellis,[64] P. R. Burchat,[64] T. S. Miyashita,[64] E. M. T. Puccio,[64] M. S. Alam,[65] J. A. Ernst,[65] R. Gorodeisky,[66] N. Guttman,[66] D. R. Peimer,[66] A. Soffer,[66] S. M. Spanier,[67] J. L. Ritchie,[68] A. M. Ruland,[68] R. F. Schwitters,[68] B. C. Wray,[68] J. M. Izen,[69] X. C. Lou,[69] F. Bianchi,[70a,70b] F. De Mori,[70a,70b] A. Filippi,[70a] D. Gamba,[70a,70b] S. Zambito,[70a,70b] L. Lanceri,[71a,71b] L. Vitale,[71a,71b] F. Martinez-Vidal,[72] A. Oyanguren,[72] P. Villanueva-Perez,[72] H. Ahmed,[73] J. Albert,[73] Sw. Banerjee,[73] F. U. Bernlochner,[73] H. H. F. Choi,[73] G. J. King,[73] R. Kowalewski,[73] M. J. Lewczuk,[73] T. Lueck,[73] I. M. Nugent,[73] J. M. Roney,[73] R. J. Sobie,[73] N. Tasneem,[73] T. J. Gershon,[74] P. F. Harrison,[74] T. E. Latham,[74] H. R. Band,[75] S. Dasu,[75] Y. Pan,[75] R. Prepost,[75] and S. L. Wu[75]

(*BABAR* Collaboration)

[1]*Laboratoire d'Annecy-le-Vieux de Physique des Particules (LAPP), Université de Savoie, CNRS/IN2P3, F-74941 Annecy-Le-Vieux, France*
[2]*Universitat de Barcelona, Facultat de Fisica, Departament ECM, E-08028 Barcelona, Spain*
[3a]*INFN Sezione di Bari, I-70126 Bari, Italy*
[3b]*Dipartimento di Fisica, Università di Bari, I-70126 Bari, Italy*
[4]*University of Bergen, Institute of Physics, N-5007 Bergen, Norway*
[5]*Lawrence Berkeley National Laboratory and University of California, Berkeley, California 94720, USA*
[6]*Ruhr Universität Bochum, Institut für Experimentalphysik 1, D-44780 Bochum, Germany*
[7]*University of British Columbia, Vancouver, British Columbia, Canada V6T 1Z1*
[8]*Brunel University, Uxbridge, Middlesex UB8 3PH, United Kingdom*
[9]*Budker Institute of Nuclear Physics SB RAS, Novosibirsk 630090, Russia*
[10]*University of California at Irvine, Irvine, California 92697, USA*
[11]*University of California at Riverside, Riverside, California 92521, USA*
[12]*University of California at Santa Barbara, Santa Barbara, California 93106, USA*
[13]*University of California at Santa Cruz, Institute for Particle Physics, Santa Cruz, California 95064, USA*
[14]*California Institute of Technology, Pasadena, California 91125, USA*
[15]*University of Cincinnati, Cincinnati, Ohio 45221, USA*
[16]*University of Colorado, Boulder, Colorado 80309, USA*
[17]*Colorado State University, Fort Collins, Colorado 80523, USA*
[18]*Technische Universität Dortmund, Fakultät Physik, D-44221 Dortmund, Germany*
[19]*Technische Universität Dresden, Institut für Kern- und Teilchenphysik, D-01062 Dresden, Germany*
[20]*Laboratoire Leprince-Ringuet, Ecole Polytechnique, CNRS/IN2P3, F-91128 Palaiseau, France*
[21]*University of Edinburgh, Edinburgh EH9 3JZ, United Kingdom*
[22a]*INFN Sezione di Ferrara, I-44122 Ferrara, Italy*
[22b]*Dipartimento di Fisica e Scienze della Terra, Università di Ferrara, I-44122 Ferrara, Italy*
[23]*INFN Laboratori Nazionali di Frascati, I-00044 Frascati, Italy*
[24a]*INFN Sezione di Genova, I-16146 Genova, Italy*
[24b]*Dipartimento di Fisica, Università di Genova, I-16146 Genova, Italy*
[25]*Indian Institute of Technology Guwahati, Guwahati, Assam 781 039, India*
[26]*Harvard University, Cambridge, Massachusetts 02138, USA*
[27]*Universität Heidelberg, Physikalisches Institut, Philosophenweg 12, D-69120 Heidelberg, Germany*
[28]*Humboldt-Universität zu Berlin, Institut für Physik, Newtonstraße 15, D-12489 Berlin, Germany*
[29]*Imperial College London, London, SW7 2AZ, United Kingdom*
[30]*University of Iowa, Iowa City, Iowa 52242, USA*
[31]*Iowa State University, Ames, Iowa 50011-3160, USA*
[32]*Johns Hopkins University, Baltimore, Maryland 21218, USA*
[33]*Laboratoire de l'Accélérateur Linéaire, IN2P3/CNRS et Université Paris-Sud 11, Centre Scientifique d'Orsay, B. P. 34, F-91898 Orsay Cedex, France*
[34]*Lawrence Livermore National Laboratory, Livermore, California 94550, USA*
[35]*University of Liverpool, Liverpool L69 7ZE, United Kingdom*
[36]*Queen Mary, University of London, London E1 4NS, United Kingdom*
[37]*University of London, Royal Holloway and Bedford New College, Egham, Surrey TW20 0EX, United Kingdom*
[38]*University of Louisville, Louisville, Kentucky 40292, USA*
[39]*Johannes Gutenberg-Universität Mainz, Institut für Kernphysik, D-55099 Mainz, Germany*
[40]*University of Manchester, Manchester M13 9PL, United Kingdom*
[41]*University of Maryland, College Park, Maryland 20742, USA*
[42]*Massachusetts Institute of Technology, Laboratory for Nuclear Science, Cambridge, Massachusetts 02139, USA*
[43]*McGill University, Montréal, Québec, Canada H3A 2T8*
[44a]*INFN Sezione di Milano, I-20133 Milano, Italy*
[44b]*Dipartimento di Fisica, Università di Milano, I-20133 Milano, Italy*
[45]*University of Mississippi, University, Mississippi 38677, USA*
[46]*Université de Montréal, Physique des Particules, Montréal, Québec, Canada H3C 3J7*
[47a]*INFN Sezione di Napoli, I-80126 Napoli, Italy*
[47b]*Dipartimento di Scienze Fisiche, Università di Napoli Federico II, I-80126 Napoli, Italy*
[48]*NIKHEF, National Institute for Nuclear Physics and High Energy Physics, NL-1009 DB Amsterdam, The Netherlands*
[49]*University of Notre Dame, Notre Dame, Indiana 46556, USA*
[50]*Ohio State University, Columbus, Ohio 43210, USA*
[51]*University of Oregon, Eugene, Oregon 97403, USA*
[52a]*INFN Sezione di Padova, I-35131 Padova, Italy*
[52b]*Dipartimento di Fisica, Università di Padova, I-35131 Padova, Italy*

[53]Laboratoire de Physique Nucléaire et de Hautes Energies, IN2P3/CNRS, Université Pierre et Marie Curie-Paris6, Université Denis Diderot-Paris7, F-75252 Paris, France
[54a]INFN Sezione di Perugia, I-06100 Perugia, Italy
[54b]Dipartimento di Fisica, Università di Perugia, I-06100 Perugia, Italy
[55a]INFN Sezione di Pisa, I-56127 Pisa, Italy
[55b]Dipartimento di Fisica, Università di Pisa, I-56127 Pisa, Italy
[55c]Scuola Normale Superiore di Pisa, I-56127 Pisa, Italy
[56]Princeton University, Princeton, New Jersey 08544, USA
[57a]INFN Sezione di Roma, I-00185 Roma, Italy
[57b]Dipartimento di Fisica, Università di Roma La Sapienza, I-00185 Roma, Italy
[58]Universität Rostock, D-18051 Rostock, Germany
[59]Rutherford Appleton Laboratory, Chilton, Didcot, Oxon, OX11 0QX, United Kingdom
[60]CEA, Irfu, SPP, Centre de Saclay, F-91191 Gif-sur-Yvette, France
[61]SLAC National Accelerator Laboratory, Stanford, California 94309, USA
[62]University of South Carolina, Columbia, South Carolina 29208, USA
[63]Southern Methodist University, Dallas, Texas 75275, USA
[64]Stanford University, Stanford, California 94305-4060, USA
[65]State University of New York, Albany, New York 12222, USA
[66]Tel Aviv University, School of Physics and Astronomy, Tel Aviv 69978, Israel
[67]University of Tennessee, Knoxville, Tennessee 37996, USA
[68]University of Texas at Austin, Austin, Texas 78712, USA
[69]University of Texas at Dallas, Richardson, Texas 75083, USA
[70a]INFN Sezione di Torino, I-10125 Torino, Italy
[70b]Dipartimento di Fisica Sperimentale, Università di Torino, I-10125 Torino, Italy
[71a]INFN Sezione di Trieste, I-34127 Trieste, Italy
[71b]Dipartimento di Fisica, Università di Trieste, I-34127 Trieste, Italy
[72]IFIC, Universitat de Valencia-CSIC, E-46071 Valencia, Spain
[73]University of Victoria, Victoria, British Columbia, Canada V8W 3P6
[74]Department of Physics, University of Warwick, Coventry CV4 7AL, United Kingdom
[75]University of Wisconsin, Madison, Wisconsin 53706, USA

(Received 1 April 2013; published 5 June 2013)

We search for the flavor-changing neutral-current decays $B \to K^{(*)}\nu\bar{\nu}$, and the invisible decays $J/\psi \to \nu\bar{\nu}$ and $\psi(2S) \to \nu\bar{\nu}$ via $B \to K^{(*)}J/\psi$ and $B \to K^{(*)}\psi(2S)$, respectively, using a data sample of 471×10^6 $B\bar{B}$ pairs collected by the *BABAR* experiment. We fully reconstruct the hadronic decay of one of the B mesons in the $\Upsilon(4S) \to B\bar{B}$ decay, and search for the $B \to K^{(*)}\nu\bar{\nu}$ decay in the rest of the event. We observe no significant excess of signal decays over background and report branching fraction upper limits of $\mathcal{B}(B^+ \to K^+\nu\bar{\nu}) < 3.7 \times 10^{-5}$, $\mathcal{B}(B^0 \to K^0\nu\bar{\nu}) < 8.1 \times 10^{-5}$, $\mathcal{B}(B^+ \to K^{*+}\nu\bar{\nu}) < 11.6 \times 10^{-5}$, $\mathcal{B}(B^0 \to K^{*0}\nu\bar{\nu}) < 9.3 \times 10^{-5}$, and combined upper limits of $\mathcal{B}(B \to K\nu\bar{\nu}) < 3.2 \times 10^{-5}$ and $\mathcal{B}(B \to K^*\nu\bar{\nu}) < 7.9 \times 10^{-5}$, all at the 90% confidence level. For the invisible quarkonium decays, we report branching fraction upper limits of $\mathcal{B}(J/\psi \to \nu\bar{\nu}) < 3.9 \times 10^{-3}$ and $\mathcal{B}(\psi(2S) \to \nu\bar{\nu}) < 15.5 \times 10^{-3}$ at the 90% confidence level. Using the improved kinematic resolution achieved from hadronic reconstruction, we also provide partial branching fraction limits for the $B \to K^{(*)}\nu\bar{\nu}$ decays over the full kinematic spectrum.

DOI: 10.1103/PhysRevD.87.112005 PACS numbers: 13.20.He, 13.20.Gd, 14.40.Nd

I. INTRODUCTION

Flavor-changing neutral-current transitions, such as $b \to s\nu\bar{\nu}$, are prohibited in the standard model (SM) at tree-level. However, they can occur via one-loop box or electroweak penguin diagrams, as shown in Fig. 1. They can occur also in the SM via a quarkonium resonance state $b \to sc\bar{c}$, $c\bar{c} \to \nu\bar{\nu}$, where the $c\bar{c}$ decay is mediated by a virtual Z^0 boson (Fig. 2). This latter decay process has the same final state as $b \to s\nu\bar{\nu}$ with an additional constraint from the on-shell $c\bar{c}$ mass. Both the $b \to s\nu\bar{\nu}$ and $c\bar{c} \to \nu\bar{\nu}$ decay rates are expected to be small within the SM, with

[*]Now at the University of Tabuk, Tabuk 71491, Saudi Arabia.
[†]Also with Università di Perugia, Dipartimento di Fisica, Perugia, Italy.
[‡]Now at the University of Huddersfield, Huddersfield HD1 3DH, UK.
[§]Deceased.
[‖]Now at University of South Alabama, Mobile, Alabama 36688, USA.
[¶]Also with Università di Sassari, Sassari, Italy.
[**]Now at Universidad Técnica Federico Santa Maria, Valparaiso, Chile 2390123.

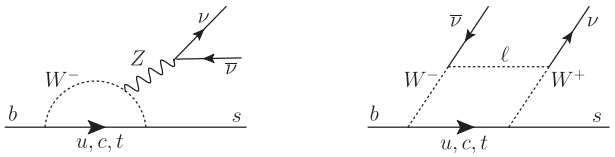

FIG. 1. Lowest-order SM Feynman diagrams for $b \to s\nu\bar{\nu}$ transitions. The virtual top quark provides the dominant contribution in each case.

branching fractions estimated to be $\mathcal{B}(B^+ \to K^+\nu\bar{\nu}) = \mathcal{B}(B^0 \to K^0\nu\bar{\nu}) = (4.5 \pm 0.7) \times 10^{-6}$, $\mathcal{B}(B^+ \to K^{*+}\nu\bar{\nu}) = \mathcal{B}(B^0 \to K^{*0}\nu\bar{\nu}) = (6.8^{+1.0}_{-1.1}) \times 10^{-6}$ [1], and $\mathcal{B}(J/\psi \to \nu\bar{\nu}) = (4.54 \times 10^{-7}) \cdot \mathcal{B}(J/\psi \to e^+e^-)$ [2]. The $b \to s\nu\bar{\nu}$ rates are predicted with smaller theoretical uncertainties than those in the corresponding $b \to s\ell^+\ell^-$ modes due to the absence of long-distance hadronic effects from electromagnetic penguin contributions.

Various new-physics scenarios exist that could significantly enhance the $b \to s\nu\bar{\nu}$ branching fractions, as well as modify the expected SM decay distributions of $s_B \equiv q^2/m_B^2$, where q^2 is the squared magnitude of the four-momentum transferred from the B meson to the neutrino pair, and m_B is the B meson mass. Some of these scenarios predict massive particles that could contribute additional loop diagrams with similar amplitudes as those in the SM, such as nonstandard Z^0 couplings with supersymmetric (SUSY) particles [1], fourth-generation quarks [3], anomalous top-charm transitions [4], or a massive U(1) gauge boson Z' [1,5]. Since $b \to s\nu\bar{\nu}$ has two final-state neutrinos, other sources of new physics can also contribute to the experimental signature of a kaon and missing four-momentum, such as low-mass dark-matter (LDM) candidates [1,6–8], unparticles [9], right-handed neutrinos [5], or SUSY particles [10]. Models with a single universal extra dimension also predict higher decay rates [11].

The decays $J/\psi \to \nu\bar{\nu}$ and $\psi(2S) \to \nu\bar{\nu}$ provide additional windows for new-physics searches. In spontaneously-broken SUSY, a $c\bar{c}$ resonance can decay into a pair of goldstinos via either a virtual Z^0 in the s-channel or a c-squark exchange in the t-channel [2] (Fig. 2). The contribution of a massive SU(2) gauge boson Z', introduced in the left-right SUSY model, could suppress the decay rates up to an order of magnitude [2].

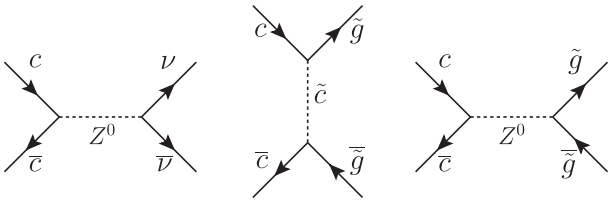

FIG. 2. Lowest-order Feynman diagrams of (from left to right) the SM decay $c\bar{c} \to \nu\bar{\nu}$, the SUSY decay $c\bar{c}$ into a pair of goldstinos ($\tilde{g}$) via a c-squark in the t-channel, and the SUSY decay $c\bar{c} \to \tilde{g}\,\tilde{\bar{g}}$ via a virtual Z^0 in the s-channel.

Conversely, a low-mass U(1) gauge boson U could enhance the invisible decay rates of quarkonium states by several orders of magnitude by coupling to LDM particles [12,13]. The U boson could decay into a pair of spin-1/2 Majorana ($\chi\chi$), spin-1/2 Dirac ($\chi\bar{\chi}$), or spin-0 ($\varphi\varphi$) LDM particles.

We search for $B \to K\nu\bar{\nu}$ and $B \to K^*\nu\bar{\nu}$, and for $J/\psi \to \nu\bar{\nu}$ and $\psi(2S) \to \nu\bar{\nu}$ via $B \to K^{(*)}J/\psi$ and $B \to K^{(*)}\psi(2S)$, respectively, where $K^{(*)}$ signifies a charged or neutral K or K^* meson [14]. We use a technique in which one B meson is exclusively reconstructed in a hadronic final state before looking for a signal decay within the rest of the event. Since the four-momentum of one B meson is fully determined, the missing mass resolution on the two final-state neutrinos and the suppression of background are improved with respect to other reconstruction techniques.

Several previous searches for $B \to K\nu\bar{\nu}$ and $B \to K^*\nu\bar{\nu}$ have been performed by both the *BABAR* and BELLE collaborations [15–19]. Currently, the most stringent published upper limits at 90% confidence level (CL) are $\mathcal{B}(B^+ \to K^+\nu\bar{\nu}) < 1.3 \times 10^{-5}$ [15] and $\mathcal{B}(B \to K^*\nu\bar{\nu}) < 8 \times 10^{-5}$ [16]. The $\mathcal{B}(B^+ \to K^+\nu\bar{\nu})$ limit was determined using semileptonic-tag reconstruction, which produces samples that are statistically larger and independent of those produced using the hadronic-tag reconstruction employed in this search. The $\mathcal{B}(B \to K^*\nu\bar{\nu})$ limit was a combination of two *BABAR* analyses, one using semileptonic-tag reconstruction and the other using hadronic-tag reconstruction.

A $J/\psi \to \nu\bar{\nu}$ search via $\psi(2S) \to \pi^+\pi^- J/\psi$ was performed by the BES collaboration, which set an upper limit at 90% CL of $\mathcal{B}(J/\psi \to \nu\bar{\nu}) < 1.2 \times 10^{-2} \cdot \mathcal{B}(J/\psi \to \mu^+\mu^-)$ [20]. This article presents the first search for $J/\psi \to \nu\bar{\nu}$ using the hadronic-tag reconstruction of a B meson decay. A search for $\psi(2S) \to \nu\bar{\nu}$ has not been performed previously.

II. THE *BABAR* DETECTOR AND DATA SAMPLE

This search uses a data sample of 471 ± 3 million $B\bar{B}$ pairs, corresponding to an integrated luminosity of 429 fb^{-1} collected at the $\Upsilon(4S)$ resonance [21]. The data were recorded with the *BABAR* detector [22] at the PEP-II asymmetric-energy e^+e^- storage rings. The charged-particle tracking system consists of a five-layer double-sided silicon vertex tracker and a 40-layer drift chamber, both coaxial with a 1.5 T solenoidal magnetic field. Charged kaons and pions are distinguished by specific ionization energy-loss measurements from the tracking system for lower momentum particles, and by measurements from a ring-imaging Cherenkov radiation detector for higher momentum particles. A CsI(Tl) electromagnetic calorimeter is used to reconstruct photons of energy greater than 20 MeV and to identify electrons. Muon identification is provided by the instrumented flux return of the magnet. Particle identification (PID)

algorithms are trained to identify charged particle types by using 36 input parameters including momentum, polar and azimuthal angles, the Cherenkov angle, and energy-loss measurements [23]. We employ PID criteria that select K^+ mesons with an efficiency greater than 85% and with approximately 1% misidentification probability for pions and muons.

Signal and background decays are studied using Monte Carlo (MC) samples simulated with Geant4 [24]. The simulation includes a detailed model of the *BABAR* detector geometry and response. Beam-related background and detector noise are extracted from data and are overlaid on the MC simulated events. Large MC samples of generic $B\bar{B}$ and continuum ($e^+e^- \to \tau^+\tau^-$ or $e^+e^- \to q\bar{q}$, where $q = u,\ d,\ s,\ c$) events provide ten times the number of $\Upsilon(4S) \to B\bar{B}$ and $e^+e^- \to c\bar{c}$ events as in the data sample, and four times the number of other continuum decays. The $\Upsilon(4S) \to B\bar{B}$ signal MC samples are generated with one B meson decaying via $B \to K^{(*)}\nu\bar{\nu}$, with and without the $c\bar{c}$ resonances, while the other B meson decays according to a model tuned to world averages of allowed decay channels. The s_B distributions for $B \to K^{(*)}\nu\bar{\nu}$ decays within signal MC samples are generated initially using a phase-space model, and then reweighted using the model from Ref. [1], henceforth referred to as ABSW. Within $B \to K^*\nu\bar{\nu}$ decays, this model is also used to reweight the helicity-angle distribution between the signal B and the K^+ or K^0 flight directions in the K^* rest frame. The helicity amplitudes for the decay channels $B \to K^*J/\psi$ and $B \to K^*\psi(2S)$ are generated using values taken from a *BABAR* measurement [25].

III. ANALYSIS METHOD

Event selection for both the $B \to K^{(*)}\nu\bar{\nu}$ and $B \to K^{(*)}c\bar{c}$, $c\bar{c} \to \nu\bar{\nu}$ searches begins by fully reconstructing a B meson ($B_{\rm tag}$) in one of many hadronic final states, $\bar{B} \to SX^-_{\rm had}$, where S is a "seed" meson ($D^{(*)+}$, $D^{(*)0}$, $D_s^{(*)+}$, or J/ψ) and $X^-_{\rm had}$ is a collection of at most five mesons, composed of charged and neutral kaons and pions with a net charge of -1. This method, which was used also in Ref. [26], reconstructs additional modes with respect to previous hadronic-tag $B \to K^{(*)}\nu\bar{\nu}$ analyses [16,17], and results in approximately twice the reconstruction efficiency. The D seeds are reconstructed in the decay modes $D^+ \to K^0_S\pi^+$, $K^0_S\pi^+\pi^0$, $K^0_S\pi^+\pi^+\pi^-$, $K^-\pi^+\pi^+$, $K^-\pi^+\pi^+\pi^0$, $K^+K^-\pi^+$, $K^+K^-\pi^+\pi^0$; $D^0 \to K^-\pi^+$, $K^-\pi^+\pi^0$, $K^-\pi^+\pi^+\pi^-$, $K^0_S\pi^+\pi^-$, $K^0_S\pi^+\pi^-\pi^0$, K^+K^-, $\pi^+\pi^-$, $\pi^+\pi^-\pi^0$, and $K^0_S\pi^0$. Additional seeds are reconstructed as $D^{*+} \to D^0\pi^+$, $D^+\pi^0$; $D^{*0} \to D^0\pi^0$, $D^0\gamma$; $D_s^{*+} \to D_s^+\gamma$; $D_s^+ \to \phi[\to K^+K^-]\pi^+$, $K^0_SK^+$; and $J/\psi \to e^+e^-$, $\mu^+\mu^-$. The K^0_S candidates are reconstructed via their decay to $\pi^+\pi^-$.

Well-reconstructed $B_{\rm tag}$ candidates are selected using two kinematic variables: $\Delta E = E_{B_{\rm tag}} - \sqrt{s}/2$ and $m_{\rm ES} = \sqrt{s/4 - \vec{p}^{\,2}_{B_{\rm tag}}}$, where $E_{B_{\rm tag}}$ and $\vec{p}_{B_{\rm tag}}$ are the energy and momentum vector of the $B_{\rm tag}$ candidate, respectively, in the e^+e^- center-of-mass (CM) frame and $\sqrt{s}$ is the total energy of the e^+e^- system. The value of ΔE, which peaks at zero for correctly reconstructed B mesons, is required to be between -0.12 and 0.12 GeV or within two standard deviations around the mean for a given $X^-_{\rm had}$ mode, whichever is the tighter constraint. If more than one $B_{\rm tag}$ candidate is reconstructed, the one in the mode with the highest purity (fraction of candidates that are correctly reconstructed within a given $B_{\rm tag}$ decay mode) is chosen. If there are multiple candidates with the same purity, the one with the smallest $|\Delta E|$ is selected.

After requiring that the event contains between one and three charged tracks not used in the $B_{\rm tag}$ reconstruction ("signal-side" tracks), the purity of each mode is recalculated, and only the $B_{\rm tag}$ modes that have a recalculated purity greater than 68% are retained. This results in a total of 448 final states. This purity value was optimized by maximizing the figure of merit [27]

$$\frac{\varepsilon_i^{\rm sig}}{\frac{1}{2}n_\sigma + \sqrt{N_i^{\rm bkg}}}, \tag{1}$$

where the number of sigmas $n_\sigma = 1.28$ corresponds to a one-sided Gaussian limit at 90% CL, $\varepsilon_i^{\rm sig}$ is the total signal efficiency, and $N_i^{\rm bkg}$ is the expected number of background events, with i representing one of the signal decay channels. All other selection criteria discussed henceforth were optimized simultaneously using this same figure of merit.

The signal region of the $B_{\rm tag}$ candidate is defined as $5.273 < m_{\rm ES} < 5.290$ GeV/c^2 (Fig. 3), since correctly reconstructed B mesons produce a peak in this region near the nominal B-meson mass. The $B_{\rm tag}$ candidates that are incorrectly reconstructed ("combinatorial" events), which result from continuum events or are due to particles assigned to the wrong B meson, produce a distribution that is relatively uniform below the $m_{\rm ES}$ signal region and decreases toward the kinematic limit within it. Approximately 0.3% of signal MC events and 12.0 million data events contain a $B_{\rm tag}$ that is reconstructed using the above requirements and found to be within the $m_{\rm ES}$ signal region.

Since B mesons are spin zero and are produced with low momentum in the CM frame (~ 0.32 GeV/c), their decay products are more isotropically distributed than non-$B\bar{B}$ background. For example, $|\cos\theta_{\rm T}|$, where $\theta_{\rm T}$ is the angle in the CM frame between the $B_{\rm tag}$ thrust [28] axis and the thrust axis of all other particles in the event, has a uniform distribution for $B\bar{B}$ events but peaks near one for continuum events. Continuum background is suppressed by using a multivariate likelihood selector based on six event-shape variables. These consist of $|\cos\theta_{\rm T}|$, the cosine of the angle between $\vec{p}_{B_{\rm tag}}$ and the beam axis, the magnitude of the $B_{\rm tag}$

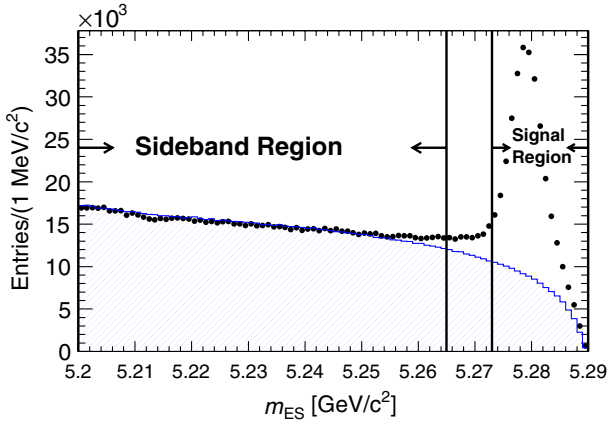

FIG. 3 (color online). The $m_{\rm ES}$ distribution for the $B_{\rm tag}$ candidates in data (points) and in the expected combinatorial background as predicted by the MC (shaded). This distribution includes only the charged and neutral $B_{\rm tag}$ candidates that pass the purity restrictions, the multivariate continuum suppression, and a requirement of one to three signal-side tracks. The data within the $m_{\rm ES}$ sideband region is used to extrapolate the expected number of combinatorial background events within the signal region.

thrust, the component of the $B_{\rm tag}$ thrust along the beam axis, the angle between the missing momentum vector ($\vec{p}_{\rm miss}$) and the beam axis, and the ratio of the second-to-zeroth Fox-Wolfram moment [29] computed using all charged and neutral particles in the event. The multivariate selector requires

$$\mathcal{L}_B \equiv \frac{\prod_j \mathcal{P}_B(x_j)}{\prod_j \mathcal{P}_B(x_j) + \prod_j \mathcal{P}_q(x_j)} > 53\%, \qquad (2)$$

where $\mathcal{P}_q(x_j)$ and $\mathcal{P}_B(x_j)$ are probability density functions determined from MC that describe continuum and signal-like $B\bar{B}$ events, respectively, for the six event-shape variables x_j. The $\mathcal{L}_B$ requirement, which was optimized with other selection criteria using Eq. (1), also improves the agreement between data and MC by suppressing unmodeled continuum backgrounds.

In the sample of selected $B_{\rm tag}$ candidates, signal events are chosen such that a single $K^{(*)}$ candidate can be reconstructed within the rest of the event and no additional charged tracks remain in the event. The sum of the $K^{(*)}$ and $B_{\rm tag}$ candidate charges must equal zero. Since signal decays have two final-state neutrinos, these events are required to have missing energy greater than zero, where the missing energy is defined as the CM energy minus all detected calorimeter deposits from charged and neutral particles in the event. For $B \to K^{(*)}\nu\bar{\nu}$, the signal decays are reconstructed in six channels: $B^+ \to K^+\nu\bar{\nu}$; $B^0 \to K^0\nu\bar{\nu}$ where $K^0 \to K^0_S$; $B^+ \to K^{*+}\nu\bar{\nu}$, where $K^{*+} \to K^+\pi^0$ and $K^{*+} \to K^0_S\pi^+$; and $B^0 \to K^{*0}\nu\bar{\nu}$, where $K^{*0} \to K^+\pi^-$ and $K^{*0} \to K^0_S\pi^0$. For $c\bar{c} \to \nu\bar{\nu}$, the same six signal channels are employed with an additional requirement that the $K^{(*)}$ momentum is consistent with a two-body decay, either $B \to K^{(*)}J/\psi$ or $B \to K^{(*)}\psi(2S)$. The J/ψ and $\psi(2S)$ mesons then decay into a pair of neutrinos, thus yielding the same final states as for $B \to K^{(*)}\nu\bar{\nu}$.

We reconstruct $K^0_S \to \pi^+\pi^-$ decay candidates using two tracks of opposite charge, which originate from a common vertex and produce an invariant mass within ± 7 MeV/c^2 of the nominal K^0_S mass [30]. The PID for each track must be inconsistent with that for an electron, muon, or kaon. The π^0 candidates are reconstructed from pairs of photon candidates with individual energies greater than 30 MeV, a total CM energy greater than 200 MeV, and a $\gamma\gamma$ invariant mass between 100 and 160 MeV/c^2. All K^+ candidates must satisfy the PID criteria for a kaon.

Reconstructed K^* candidates are required to have an invariant mass within ± 70 MeV/c^2 of the nominal K^* mass [30]. A $K^{*+} \to K^0_S\pi^+$ candidate combines a K^0_S candidate with a track that satisfies the PID criteria for a pion. If more than one $K^{*+} \to K^0_S\pi^+$ candidate can be reconstructed in an event, the one with the mass closest to the nominal K^{*+} mass is chosen. A $K^{*0} \to K^+\pi^-$ candidate combines one track that satisfies the PID criteria for a kaon with one that is inconsistent with the PID criteria for an electron, muon, or kaon. In an event containing a K^+ (K^0_S) candidate and no additional signal-side tracks, $K^* \to K^+\pi^0$ ($K^0_S\pi^0$) candidates are reconstructed if the invariant mass of a π^0 candidate and the K^+ (K^0_S) candidate falls within the K^* mass window; otherwise the event is considered for the K^+ (K^0_S) signal channel. If more than one $K^{*+} \to K^+\pi^0$ or $K^{*0} \to K^0_S\pi^0$ candidate can be reconstructed, the one with the highest energy π^0 candidate is chosen.

Once the $B_{\rm tag}$ and $K^{(*)}$ are identified, the signal events are expected to contain little or no additional energy within the calorimeter. However, additional energy deposits can result from beam-related photons, hadronic shower fragments that were not reconstructed into the primary particle deposit, and photons from unreconstructed $D^* \to D\gamma/\pi^0$ transitions in the $B_{\rm tag}$ candidate. Only deposits with energy greater than 50 MeV in the rest frame of the detector are considered, and the sum of all such additional energy deposits ($E_{\rm extra}$) is required to be less than a threshold value (E_i). The values of E_i, given in Table I and depicted in Fig. 4, were optimized with the other selection criteria but

TABLE I. Threshold values E_i for the $E_{\rm extra}$ variable in each of the signal channels, determined using Eq. (1). The channels in brackets refer to the K^* decay products.

Channel	K^+	K^0	$[K^+\pi^0]$	$[K^0_S\pi^+]$	$[K^+\pi^-]$	$[K^0_S\pi^0]$
E_i [GeV]	0.11	0.28	0.18	0.29	0.31	0.33

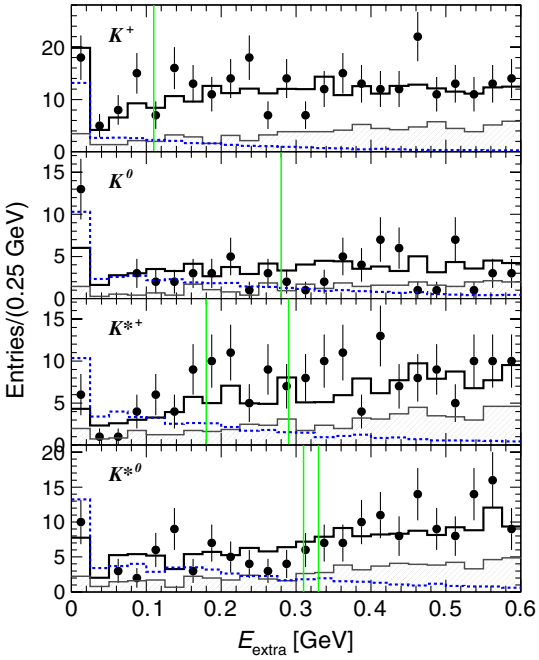

FIG. 4 (color online). The $E_{\rm extra}$ distribution over the full s_B spectrum in the (from top to bottom) K^+, K^0, K^{*+}, and K^{*0} channels after applying all other signal selection criteria. The expected combinatorial (shaded) plus $m_{\rm ES}$-peaking (solid) background contributions are overlaid on the data (points). The $B \to K^{(*)}\nu\bar{\nu}$ signal MC distributions (dashed) have arbitrary normalization. Both the $B \to K^{(*)}\nu\bar{\nu}$ and $c\bar{c} \to \nu\bar{\nu}$ searches select events to the left of the vertical line that corresponds to the E_i value of that channel, as given in Table I.

were allowed to differ between signal channels. For events within the K^+ signal channel, calorimeter deposits identified as kaon shower fragments are not included in the $E_{\rm extra}$ sum. A fragment candidate is defined as a neutral calorimeter deposit whose momentum vector, when compared to that of the signal track, is separated by polar and azimuthal angles (relative to the beam axis and in the rest frame of the detector) of $\Delta\theta$ and $\Delta\phi$, respectively, such that $r_{\rm clus} < 15°$, where $r_{\rm clus} \equiv \sqrt{(\Delta\theta)^2 + \frac{2}{3}(Q_K \cdot \Delta\phi - 8°)^2}$ and $Q_K = \pm 1$ is the $K^\pm$ charge. The $r_{\rm clus}$ and fragment candidate definitions were optimized using studies of truth information in the signal MC samples. The recovery of these kaon shower fragments improves the final signal efficiency in the K^+ channel by about 13%. This procedure was explored for the other signal tracks, but the effect was small.

The searches for $B \to K^{(*)}\nu\bar{\nu}$ and for $c\bar{c} \to \nu\bar{\nu}$ via $B \to K^{(*)}c\bar{c}$ diverge in the final step of the signal selection, which involves restricting the kinematics of the decay. The value of s_B is calculated as $(p_{B_{\rm sig}} - p_{K^{(*)}})^2/m_B^2$, where $p_{K^{(*)}}$ is the four-momentum of the $K^{(*)}$ candidate, and $p_{B_{\rm sig}}$ is the expected signal B four-momentum with an energy of $\sqrt{s}/2$, the nominal B-meson mass, and a momentum vector pointing opposite the $B_{\rm tag}$ momentum. For $B \to K^{(*)}\nu\bar{\nu}$, the signal region optimized for maximum SM sensitivity is $0 < s_B < 0.3$ for all six signal channels. This corresponds to a $K^{(*)}$ momentum greater than about 1.8 (1.7) GeV/c in the signal B rest frame for $B \to K\nu\bar{\nu}$ ($B \to K^*\nu\bar{\nu}$) events. Partial branching fractions over the full s_B spectrum are also provided for sensitivity to new-physics scenarios that modify the kinematic distributions for $B \to K^{(*)}\nu\bar{\nu}$. For $c\bar{c} \to \nu\bar{\nu}$ via $B \to K^{(*)}c\bar{c}$, the invariant mass of the two neutrinos $m_{\nu\bar{\nu}} \equiv \sqrt{s_B m_B^2}$ is expected to correspond to the mass of the J/ψ (3.097 GeV/c^2) meson or to that of the $\psi(2S)$ (3.686 GeV/c^2) meson. Signal events are selected within three standard deviations around the nominal $c\bar{c}$ masses, which results in windows of $3.044 < m_{\nu\bar{\nu}} < 3.146$ ($3.019 < m_{\nu\bar{\nu}} < 3.175$) GeV/$c^2$ for the $B \to KJ/\psi$ ($B \to K^*J/\psi$) channels, and $3.650 < m_{\nu\bar{\nu}} < 3.724$ ($3.627 < m_{\nu\bar{\nu}} < 3.739$) GeV/$c^2$ for the $B \to K\psi(2S)$ ($B \to K^*\psi(2S)$) channels.

To avoid experimenter bias, all the above selection criteria and values were optimized using the MC before looking at any data events within the $E_{\rm extra}$ and $m_{\rm ES}$ signal regions.

IV. BACKGROUND AND BRANCHING FRACTION EXTRACTION

The total number of background events $N_i^{\rm bkg}$ in the signal region has two components: $N_i^{\rm peak}$ is the number of expected background events having a correctly reconstructed $B_{\rm tag}$ candidate and hence peaking within the $m_{\rm ES}$ signal region, and $N_i^{\rm comb}$ is the number of expected combinatorial background events, including both continuum events and $B\bar{B}$ events with an incorrectly reconstructed $B_{\rm tag}$ candidate. To reduce the dependence on MC simulations, the number of $N_i^{\rm comb}$ events is extrapolated directly from the observed data events within the $m_{\rm ES}$ sideband region, defined as $5.200 < m_{\rm ES} < 5.265$ GeV/c^2 and depicted in Fig. 3. The shape of the combinatorial $m_{\rm ES}$ distribution is estimated using MC samples of continuum events and of $B\bar{B}$ events reconstructed with the wrong charge.

The number of $N_i^{\rm peak}$ events is estimated from generic $B\bar{B}$ MC samples. Over half of $N_i^{\rm peak}$ is found to be from $B \to D^{(*)}\ell\nu$ ($\ell = e$ or μ) decays in which no lepton candidate is identified in the event and the $K^{(*)}$ is a daughter of the D or D^* meson. One particular peaking background in the $B \to K^{(*)}\nu\bar{\nu}$ search is $B^+ \to \tau^+\nu_\tau$, with $\tau^+ \to K^{(*)+}\nu_\tau$, which has the same final state as the signal decay [31]. Exclusive $B^+ \to \tau^+\nu_\tau$ MC samples, assuming a branching fraction of $(1.65 \pm 0.34) \times 10^{-4}$ [30], indicate that this background constitutes less than 15 (5)% of the total background in the $B^+ \to K^+\nu\bar{\nu}$ ($B^+ \to K^{*+}\nu\bar{\nu}$) channel.

Since both $N_i^{\rm peak}$ and $\varepsilon_i^{\rm sig}$ are determined from MC samples, we normalize the MC yields to the data to account for differences between data and MC, such as from the $B_{\rm tag}$ reconstruction and the modeled branching fractions of $B_{\rm tag}$ modes within the MC. This normalization is performed before applying the full signal selection in order to have a large background-to-signal ratio; looser $K^{(*)}$ mass windows and $E_{\rm extra}$ selection requirements are used such that the number of background events is approximately 60 times larger than the final background contribution, over the full s_B spectrum. The peaking background component in the $B\bar{B}$ MC is then normalized to the number of data events that peak within the $m_{\rm ES}$ signal region. This peaking yield normalization is performed separately for charged and neutral $B_{\rm tag}$ candidates, and results in the scaling of all signal and background MC samples by 1.027 ± 0.039 (1.017 ± 0.044) for charged (neutral) $B_{\rm tag}$ candidates.

The signal branching fractions are calculated using

$$\mathcal{B}_i = \frac{N_i^{\rm obs} - (N_i^{\rm peak} + N_i^{\rm comb})}{\varepsilon_i^{\rm sig} N_{B\bar{B}}}, \qquad (3)$$

where $N_{B\bar{B}} = 471 \times 10^6$ is the total number of B meson pairs in the data sample and $N_i^{\rm obs}$ is the number of data events within the signal region. The total signal efficiency $\varepsilon_i^{\rm sig}$ includes that of the $B_{\rm tag}$ reconstruction and is determined separately for each of the signal channels i. Since misreconstructed events from other signal channels contribute to $N_i^{\rm peak}$, the branching fractions of all signal channels are determined simultaneously by inverting a 6×6 efficiency matrix ε_{ij}, which describes the probability that a signal event of process i is reconstructed in signal channel j. Branching fraction limits and uncertainties are computed using a mixed frequentist-Bayesian approach described in Ref. [32], with the systematic uncertainties on $N_i^{\rm bkg}$ and $\varepsilon_i^{\rm sig}$ modeled using Gaussian distributions. To combine the results of signal decay channels, we find the $\mathcal{B}_i$ value that maximizes a likelihood function defined as the product of the Poisson probabilities of observing $N_i^{\rm obs}$ events.

V. SYSTEMATIC STUDIES

To verify the modeling of $\varepsilon_i^{\rm sig}$ and $N_i^{\rm bkg}$, a control sample of $B \to D\ell\nu$ events is selected. In place of a signal K^* candidate, the events are required to contain a reconstructed $D^0 \to K^-\pi^+$, $D^- \to K^+\pi^-\pi^-$, or $D^- \to K_S^0\pi^-$ candidate with an invariant mass within ± 35 MeV/c^2 of the nominal D-meson mass values [30]. The event must have one additional track that satisfies the PID criteria of either an electron or muon. All other reconstruction and signal selection requirements are retained. The resulting yields in the data agree with MC expectations, assuming the well-measured branching fractions of $B \to D\ell\nu$ [30], within the 7% (12%) statistical uncertainty of the data in the $0 < s_B < 0.3$ (J/ψ or $\psi(2S)$ mass) region.

TABLE II. Summary of systematic uncertainties that are shared by the $B \to K^{(*)}\nu\bar{\nu}$, $J/\psi \to \nu\bar{\nu}$, and $\psi(2S) \to \nu\bar{\nu}$ searches. All values are relative uncertainties in %. The channels in brackets refer to the K^* decay products.

Source	K^+	$[K^+\pi^0]$	$[K_S^0\pi^+]$	K^0	$[K^+\pi^-]$	$[K_S^0\pi^0]$
$\varepsilon_i^{\rm sig}$ normalization	3.5	3.5	3.5	8.9	8.9	8.9
$N_i^{\rm bkg}$ normalization	2.3	2.3	2.3	6.0	6.0	6.0
K_S^0 reconstruction	···	···	1.4	1.4	···	1.4
K^* reconstruction	···	2.8	2.8	···	2.8	2.8
π^0 reconstruction	···	3.0	···	···	···	3.0
$E_{\rm extra}$	4.5	6.0	6.5	6.0	6.0	6.5

The control sample is used to determine the systematic uncertainties due to the MC modeling of the $E_{\rm extra}$ variable within data. Additional uncertainties on $N_i^{\rm peak}$ and $\varepsilon_i^{\rm sig}$ are due to the K_S^0 and K^* mass reconstruction windows, the π^0 reconstruction, and the uncertainties in the branching fractions [30] of the dominant backgrounds contributing to $N_i^{\rm peak}$. The uncertainty on $N_i^{\rm comb}$ is dominated by the sideband data statistics. Other systematic uncertainties, such as those from PID, tracking, $B_{\rm tag}$ reconstruction, $N_{B\bar{B}}$, and the assumption that charged and neutral $B\bar{B}$ pairs are produced at equal rates, are all accounted for by the normalization of the MC peaking yields. Because the peaking yield in data depends on the extrapolated shape of the combinatorial $B_{\rm tag}$ background, the normalization scale factors are

TABLE III. Summary of systematic uncertainties that differ between the $B \to K^{(*)}\nu\bar{\nu}$, $J/\psi \to \nu\bar{\nu}$, and $\psi(2S) \to \nu\bar{\nu}$ searches, and the total systematic uncertainties for each signal channel. All values are relative uncertainties in %. The total systematic uncertainties are determined by adding in quadrature each relevant uncertainty, including those listed in Table II.

Source	K^+	$[K^+\pi^0]$	$[K_S^0\pi^+]$	K^0	$[K^+\pi^-]$	$[K_S^0\pi^0]$
			$B \to K^{(*)}\nu\bar{\nu}$			
$N_i^{\rm peak}$ $\mathcal{B}$'s	2.8	2.8	2.8	2.8	2.8	2.8
s_B resolution	3.6	3.6	3.6	3.6	3.6	3.6
Total $N_i^{\rm peak}$ syst.	6.8	8.9	8.8	9.7	10.0	10.9
Total $N_i^{\rm comb}$ syst.	2.3	2.3	2.3	6.0	6.0	6.0
Total $\varepsilon_i^{\rm sig}$ syst.	6.7	8.8	8.8	11.4	11.7	12.4
			$J/\psi \to \nu\bar{\nu}$			
$N_i^{\rm peak}$ $\mathcal{B}$'s	3.5	3.5	3.5	3.5	3.5	3.5
$m_{\nu\bar{\nu}}$ resolution	1.1	2.1	0.4	0.7	0.3	1.3
Total $N_i^{\rm peak}$ syst.	6.2	8.6	8.4	9.3	9.6	10.5
Total $N_i^{\rm comb}$ syst.	2.3	2.3	2.3	6.0	6.0	6.0
Total $\varepsilon_i^{\rm sig}$ syst.	5.8	8.3	8.0	10.8	11.1	11.9
			$\psi(2S) \to \nu\bar{\nu}$			
$N_i^{\rm peak}$ $\mathcal{B}$'s	2.8	2.8	2.8	2.8	2.8	2.8
$m_{\nu\bar{\nu}}$ resolution	0.8	2.4	1.0	0.9	1.8	3.1
Total $N_i^{\rm peak}$ syst.	5.8	8.5	8.1	9.1	9.5	10.7
Total $N_i^{\rm comb}$ syst.	2.3	2.3	2.3	6.0	6.0	6.0
Total $\varepsilon_i^{\rm sig}$ syst.	5.8	8.4	8.1	10.9	11.2	12.2

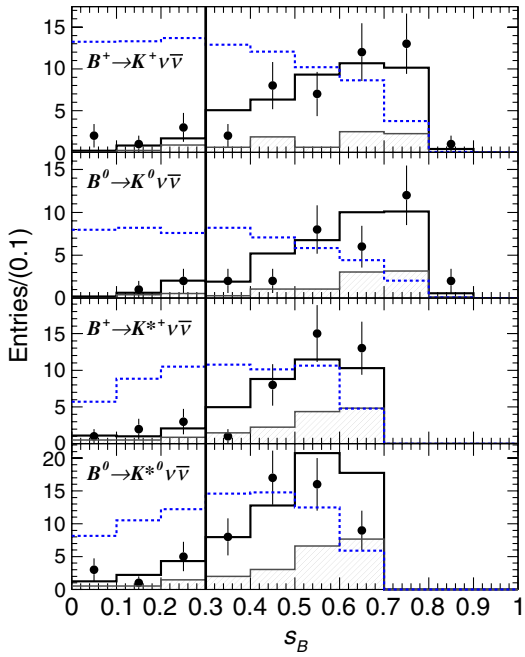

FIG. 5 (color online). The s_B distribution for (from top to bottom) $B^+ \to K^+\nu\bar{\nu}$, $B^0 \to K^0\nu\bar{\nu}$, $B^+ \to K^{*+}\nu\bar{\nu}$, and $B^0 \to K^{*0}\nu\bar{\nu}$ events after applying the full signal selection. The expected combinatorial (shaded) plus $m_{\rm ES}$-peaking (solid) background contributions are overlaid on the data (points). The signal MC distributions (dashed) are normalized to branching fractions of 20×10^{-5} for $B^+ \to K^+\nu\bar{\nu}$ and 50×10^{-5} for the other channels. Events to the left of the vertical lines are selected to obtain SM-sensitive limits, while the full spectra are used to determine partial branching fractions.

re-evaluated by varying the method used to extrapolate this shape. The resulting variations on the final $N_i^{\rm bkg}$ and $\varepsilon_i^{\rm sig}$ values are taken as the systematic uncertainties due to the normalization.

Due to the approximately 1.0% resolution on the s_B measurement around $s_B = 0.3$, an uncertainty is evaluated within the $B \to K^{(*)}\nu\bar{\nu}$ signal region. Similarly, the resolution on $m_{\nu\bar{\nu}}$ contributes to uncertainties within the $J/\psi \to \nu\bar{\nu}$ and $\psi(2S) \to \nu\bar{\nu}$ signal regions. Only the systematic uncertainties due to the $N_i^{\rm peak}$ branching fractions and to s_B or $m_{\nu\bar{\nu}}$ differ between the $B \to K^{(*)}\nu\bar{\nu}$, $J/\psi \to \nu\bar{\nu}$, and $\psi(2S) \to \nu\bar{\nu}$ searches. The systematic uncertainties are summarized in Tables II and III; the former lists the uncertainties shared by the searches, while the latter lists those that differ.

VI. RESULTS FOR $B \to K^{(*)}\nu\bar{\nu}$

Figure 5 shows the observed data yields, expected background contributions, and SM signal distributions over the full s_B spectrum. Tables IV and V summarize the number of observed data events within the s_B signal region ($0 < s_B < 0.3$), expected backgrounds, $B \to K^{(*)}\nu\bar{\nu}$ signal efficiencies, branching fraction central values, and branching fraction limits at the 90% CL. Combining the signal channels, we determine upper limits of $\mathcal{B}(B \to K\nu\bar{\nu}) < 3.2 \times 10^{-5}$ and $\mathcal{B}(B \to K^*\nu\bar{\nu}) < 7.9 \times 10^{-5}$. Since we see a small excess over the expected background in the K^+ channel, we report a two-sided 90% confidence interval. However, the probability of observing such an excess within the signal region, given the uncertainty on the background, is 8.4% which corresponds to a one-sided Gaussian significance of about 1.4σ. Therefore, this excess is not considered significant.

Using the same procedure as when combining signal decay channels, the $B \to K\nu\bar{\nu}$ branching fraction central values are combined with a previous semileptonic-tag *BABAR* analysis that searched within a statistically independent data sample [15]. We obtain combined *BABAR* upper limits at the 90% CL of

$$\begin{aligned} \mathcal{B}(B^+ \to K^+\nu\bar{\nu}) &< 1.6 \times 10^{-5}, \\ \mathcal{B}(B^0 \to K^0\nu\bar{\nu}) &< 4.9 \times 10^{-5}, \quad \text{and} \\ \mathcal{B}(B \to K\nu\bar{\nu}) &< 1.7 \times 10^{-5}. \end{aligned} \tag{4}$$

The combined central value is $\mathcal{B}(B \to K\nu\bar{\nu}) = (0.8^{+0.7}_{-0.6}) \times 10^{-5}$, where the uncertainty includes both

TABLE IV. Expected $B \to K^*\nu\bar{\nu}$ background yields $N_i^{\rm bkg} = N_i^{\rm peak} + N_i^{\rm comb}$, signal efficiencies $\varepsilon_i^{\rm sig}$, number of observed data events $N_i^{\rm obs}$, resulting branching fraction upper limits at 90% CL, and the combined upper limits and central values, all within the $0 < s_B < 0.3$ region. Uncertainties are statistical and systematic, respectively. The channels in brackets refer to the K^* decay products.

	$B^+ \to [K^+\pi^0]\nu\bar{\nu}$	$B^+ \to [K^0_S\pi^+]\nu\bar{\nu}$	$B^0 \to [K^+\pi^-]\nu\bar{\nu}$	$B^0 \to [K^0_S\pi^0]\nu\bar{\nu}$
$N_i^{\rm peak}$	$1.2 \pm 0.4 \pm 0.1$	$1.3 \pm 0.4 \pm 0.1$	$5.0 \pm 0.8 \pm 0.5$	$0.2 \pm 0.2 \pm 0.0$
$N_i^{\rm comb}$	$1.1 \pm 0.4 \pm 0.0$	$0.8 \pm 0.3 \pm 0.0$	$2.0 \pm 0.5 \pm 0.1$	$0.5 \pm 0.3 \pm 0.0$
$N_i^{\rm bkg}$	$2.3 \pm 0.5 \pm 0.1$	$2.0 \pm 0.5 \pm 0.1$	$7.0 \pm 0.9 \pm 0.5$	$0.7 \pm 0.3 \pm 0.0$
$\varepsilon_i^{\rm sig}$ $(\times 10^{-5})$	$4.9 \pm 0.2 \pm 0.4$	$6.0 \pm 0.2 \pm 0.5$	$12.2 \pm 0.3 \pm 1.4$	$1.2 \pm 0.1 \pm 0.1$
$N_i^{\rm obs}$	3	3	7	2
Limit	$<19.4 \times 10^{-5}$	$<17.0 \times 10^{-5}$	$<8.9 \times 10^{-5}$	$<86 \times 10^{-5}$
$\mathcal{B}(B^{+/0} \to K^{*+/0}\nu\bar{\nu})$	$(3.3^{+6.2+1.7}_{-3.6-1.3}) \times 10^{-5}$		$(2.0^{+5.2+2.0}_{-4.3-1.7}) \times 10^{-5}$	
Limit	$<11.6 \times 10^{-5}$		$<9.3 \times 10^{-5}$	
$\mathcal{B}(B \to K^*\nu\bar{\nu})$	$(2.7^{+3.8+1.2}_{-2.9-1.0}) \times 10^{-5}$			
Limit	$<7.9 \times 10^{-5}$			

TABLE V. Expected $B \to K\nu\bar{\nu}$ background yields $N_i^{\rm bkg} = N_i^{\rm peak} + N_i^{\rm comb}$, signal efficiencies $\varepsilon_i^{\rm sig}$, number of observed data events $N_i^{\rm obs}$, resulting branching fraction upper limits at 90% CL, the central values $\mathcal{B}_i$, and the combined upper limits and central value, all within the $0 < s_B < 0.3$ region. Lower limits at 90% CL are also reported, as discussed in the text. Uncertainties are statistical and systematic, respectively. The $B^0 \to K^0\nu\bar{\nu}$ efficiency accounts for $\mathcal{B}(K^0 \to K_S^0)$ and $\mathcal{B}(K_S^0 \to \pi^+\pi^-)$ [30].

	$B^+ \to K^+\nu\bar{\nu}$	$B^0 \to K^0\nu\bar{\nu}$
$N_i^{\rm peak}$	$1.8 \pm 0.4 \pm 0.1$	$2.0 \pm 0.5 \pm 0.2$
$N_i^{\rm comb}$	$1.1 \pm 0.4 \pm 0.0$	$0.9 \pm 0.4 \pm 0.1$
$N_i^{\rm bkg}$	$2.9 \pm 0.6 \pm 0.1$	$2.9 \pm 0.6 \pm 0.2$
$\varepsilon_i^{\rm sig}$ $(\times 10^{-5})$	$43.8 \pm 0.7 \pm 3.0$	$10.3 \pm 0.2 \pm 1.2$
$N_i^{\rm obs}$	6	3
$\mathcal{B}_i$	$(1.5^{+1.7+0.4}_{-0.8-0.2}) \times 10^{-5}$	$(0.14^{+6.0+1.7}_{-1.9-0.9}) \times 10^{-5}$
Limits	$(>0.4, <3.7) \times 10^{-5}$	$<8.1 \times 10^{-5}$
$\mathcal{B}(B \to K\nu\bar{\nu})$	$(1.4^{+1.4+0.3}_{-0.9-0.2}) \times 10^{-5}$	
Limits	$(>0.2, <3.2) \times 10^{-5}$	

statistical and systematic uncertainties. These combined results reweight the s_B distribution to that of the ABSW theoretical model (dashed curve in Fig. 5), which decreases the signal efficiencies published in Ref. [15] by approximately 10%. The $B \to K^*\nu\bar{\nu}$ central values also can be combined with the semileptonic-tag results from a previous *BABAR* search [16]. In order to obtain approximate frequentist intervals, the likelihood functions in the previous search are extended to include possibly negative signals. We obtain combined *BABAR* upper limits at the 90% CL of

$$\begin{aligned} \mathcal{B}(B^+ \to K^{*+}\nu\bar{\nu}) &< 6.4 \times 10^{-5}, \\ \mathcal{B}(B^0 \to K^{*0}\nu\bar{\nu}) &< 12 \times 10^{-5}, \quad \text{and} \\ \mathcal{B}(B \to K^*\nu\bar{\nu}) &< 7.6 \times 10^{-5}. \end{aligned} \tag{5}$$

The combined central value is $\mathcal{B}(B \to K^*\nu\bar{\nu}) = (3.8^{+2.9}_{-2.6}) \times 10^{-5}$.

Since certain new-physics models suggest that enhancements are possible at high s_B values, we also report model-independent partial branching fractions ($\Delta\mathcal{B}_i$) over the full s_B spectrum by removing the low-s_B requirement. The $\Delta\mathcal{B}_i$ values are calculated in intervals of $s_B = 0.1$, using Eq. (3) (with the $N_i^{\rm obs}$, $N_i^{\rm peak}$, $N_i^{\rm comb}$, and $\varepsilon_i^{\rm sig}$ values found within the given interval) multiplied by the fraction of the signal efficiency distribution inside that interval. Figure 6 shows the partial branching fractions. The signal efficiency distributions are relatively independent of s_B, which are also illustrated in Fig. 6. To compute model-specific values from these results, one can sum the central values within the model's dominant interval(s) (with uncertainties added in quadrature) and divide the sum by the fraction of the model's distribution that is expected to lie within the same s_B intervals. These partial branching fractions provide

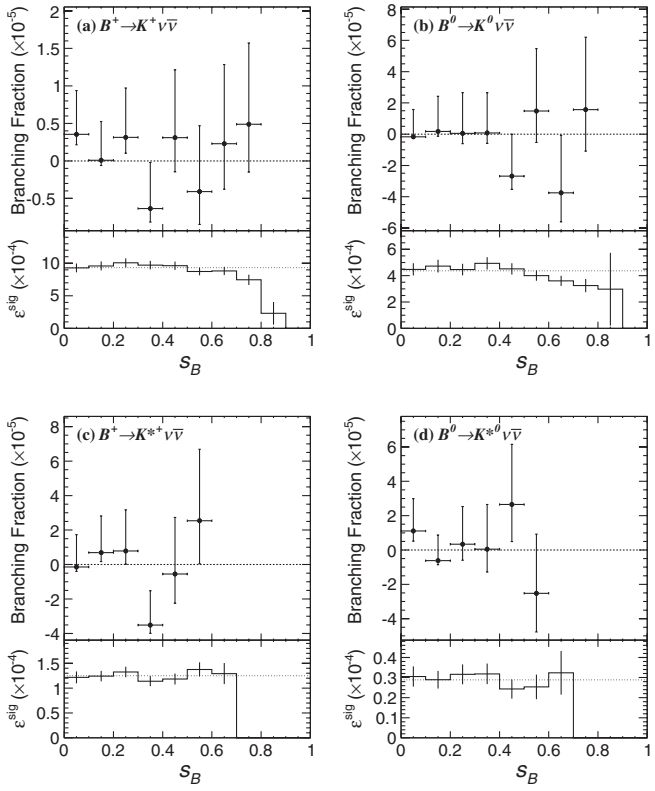

FIG. 6. The central values (points with 1σ error bars) of the partial branching fractions $\Delta\mathcal{B}_i$ versus s_B, for (a) $B^+ \to K^+\nu\bar{\nu}$, (b) $B^0 \to K^0\nu\bar{\nu}$, (c) $B^+ \to K^{*+}\nu\bar{\nu}$, and (d) $B^0 \to K^{*0}\nu\bar{\nu}$. The subplots show the distribution of the final signal efficiencies within each s_B interval (histogram with error bars) and over the full s_B spectra (dotted line). The partial branching fractions are provided only within the intervals that are unaffected by the kinematic limit at large s_B.

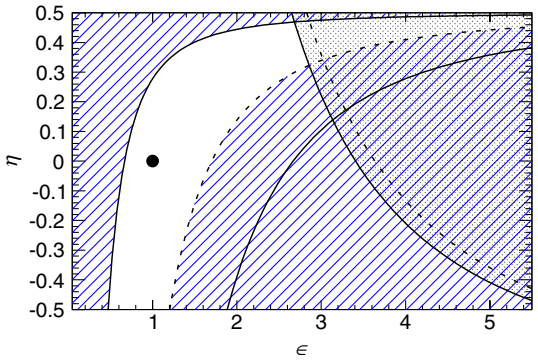

FIG. 7 (color online). The constraints at 90% CL on ϵ and η of Eq. (6) for sensitivity to new physics with right-handed currents. The $B \to K\nu\bar{\nu}$ (diagonal shading) and $B \to K^*\nu\bar{\nu}$ (grey shading) excluded areas are determined from the upper and lower limits of this $B \to K^{(*)}\nu\bar{\nu}$ analysis (solid curves) and from the most-stringent upper limits from previous semileptonic-tag analyses [15,16] (dashed curves). The dot shows the expected SM value.

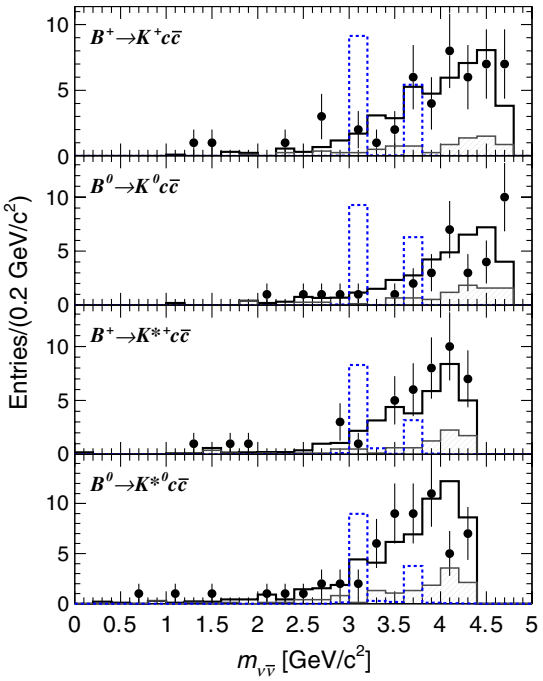

FIG. 8 (color online). The $m_{\nu\bar{\nu}} \equiv \sqrt{s_B m_B^2}$ distribution for (from top to bottom) $B^+ \to K^+ c\bar{c}$, $B^0 \to K^0 c\bar{c}$, $B^+ \to K^{*+} c\bar{c}$, and $B^0 \to K^{*0} c\bar{c}$ events after applying the full signal selection. The expected combinatorial (shaded) plus $m_{\rm ES}$-peaking (solid) background contributions are overlaid on the data (points). The signal MC distributions (dashed) are normalized to $\mathcal{B}(c\bar{c} \to \nu\bar{\nu})$ values of 2% for the K^+ channel, 10% for the K^0 channel, and 5% for the K^* channels.

branching fraction upper limits for several new-physics scenarios at the level of 10^{-5}.

The $B \to K^{(*)}\nu\bar{\nu}$ decays are also sensitive to the short-distance Wilson coefficients $|C_{L,R}^{\nu}|$ for the left- and right-handed weak currents, respectively. These couple two quarks to two neutrinos via an effective field theory point interaction [33]. Although $|C_R^{\nu}| = 0$ within the SM, right-handed currents from new physics, such as non-SM Z^0 penguin couplings, could produce nonzero values. Using the parameterization from Ref. [1],

$$\epsilon \equiv \frac{\sqrt{|C_L^{\nu}|^2 + |C_R^{\nu}|^2}}{|C_{L,\rm SM}^{\nu}|}, \qquad \eta \equiv \frac{-\mathrm{Re}(C_L^{\nu} C_R^{\nu *})}{|C_L^{\nu}|^2 + |C_R^{\nu}|^2}, \tag{6}$$

the $B \to K^* \nu\bar{\nu}$ upper limits from this search improve the constraints from previous searches on the Wilson-coefficient parameter space, as shown in Fig. 7. The $B \to K\nu\bar{\nu}$ lower limit provides the first upper bound on η and lower bound on ϵ. These constraints are consistent with the expected SM values of $\epsilon = 1$ and $\eta = 0$.

VII. RESULTS FOR $c\bar{c} \to \nu\bar{\nu}$

In the search for $c\bar{c} \to \nu\bar{\nu}$, Fig. 8 shows the $m_{\nu\bar{\nu}}$ distribution of the observed data yields, expected background contributions, and SM signal distributions. Tables VI and VII summarize the background contribution values and signal efficiencies within the J/ψ and $\psi(2S)$ invariant mass regions. The tables also report the combined branching fraction central values and the branching fraction upper limits at 90% CL for $J/\psi \to \nu\bar{\nu}$ and $\psi(2S) \to \nu\bar{\nu}$. The signal efficiencies account for the $B \to K^{(*)} J/\psi$ and $B \to K^{(*)}\psi(2S)$ branching fractions and their errors, which are taken from Ref. [30]. The data yield is consistent with zero observed $c\bar{c} \to \nu\bar{\nu}$ signal events in all channels.

The combined upper limits for the charmonium branching fraction values are determined to be

$$\frac{\mathcal{B}(J/\psi \to \nu\bar{\nu})}{\mathcal{B}(J/\psi \to e^+e^-)} < 6.6 \times 10^{-2} \quad \text{and} \quad \frac{\mathcal{B}(\psi(2S) \to \nu\bar{\nu})}{\mathcal{B}(\psi(2S) \to e^+e^-)} < 2.0, \tag{7}$$

where $\mathcal{B}(J/\psi \to e^+e^-)$ and $\mathcal{B}(\psi(2S) \to e^+e^-)$ are taken from Ref. [30]. With the addition of a new-physics U boson, these ratios would be proportional to $|f_{cV} c_{\chi,\varphi}|$, where $c_{\chi,\varphi}$ and f_{cV} are the U couplings to the LDM particles χ or φ and to the c-quark respectively [13]. The J/ψ decay ratio yields upper limits at 90% CL of $|f_{cV} c_{\chi,\varphi}| < (3.0, 2.1, 1.5) \times 10^{-2}$ for spin-1/2 Majorana and spin-1/2 Dirac LDM particles, respectively. These

TABLE VI. Expected $J/\psi \to \nu\bar{\nu}$ background yields $N_i^{\rm peak}$ and $N_i^{\rm bkg}$, signal efficiencies $\varepsilon_i^{\rm sig}$, number of observed data events $N_i^{\rm obs}$, and the resulting branching fraction central value and upper limit at 90% CL, all within the $m_{\nu\bar{\nu}}$ invariant mass region corresponding to the J/ψ mass. Uncertainties are statistical and systematic, respectively. The $N_i^{\rm comb}$ yields are calculable as $N_i^{\rm bkg} - N_i^{\rm peak}$.

	$J/\psi \to \nu\bar{\nu}$					
Channel	K^+	K^0	$K^{*+} \to K^+\pi^0$	$K^{*+} \to K_S^0\pi^+$	$K^{*0} \to K^+\pi^-$	$K^{*0} \to K_S^0\pi^0$
$N_i^{\rm peak}$	$0.4 \pm 0.2 \pm 0.0$	$0.7 \pm 0.3 \pm 0.1$	$0.8 \pm 0.3 \pm 0.1$	$0.4 \pm 0.2 \pm 0.0$	$2.6 \pm 0.5 \pm 0.3$	$0.6 \pm 0.2 \pm 0.1$
$N_i^{\rm bkg}$	$0.5 \pm 0.2 \pm 0.0$	$0.7 \pm 0.3 \pm 0.1$	$0.8 \pm 0.3 \pm 0.1$	$0.8 \pm 0.3 \pm 0.0$	$2.8 \pm 0.5 \pm 0.3$	$0.6 \pm 0.2 \pm 0.1$
$\varepsilon_i^{\rm sig}$ $(\times 10^{-8})$	$95.3 \pm 4.4 \pm 5.5$	$19.3 \pm 1.0 \pm 2.1$	$20.9 \pm 1.5 \pm 1.7$	$12.4 \pm 0.8 \pm 1.0$	$36.2 \pm 1.9 \pm 4.0$	$1.8 \pm 0.2 \pm 0.2$
$N_i^{\rm obs}$	1	0	1	0	0	1
$\mathcal{B}(J/\psi \to \nu\bar{\nu})$			$(0.2^{+2.7+0.5}_{-0.9-0.4}) \times 10^{-3}$			
Limit			$<3.9 \times 10^{-3}$			

TABLE VII. Expected $\psi(2S) \to \nu\bar{\nu}$ background yields $N_i^{\rm peak}$ and $N_i^{\rm bkg}$, signal efficiencies $\varepsilon_i^{\rm sig}$, number of observed data events $N_i^{\rm obs}$, and the resulting branching fraction central value and upper limit at 90% CL, all within the $m_{\nu\bar{\nu}}$ invariant mass region corresponding to the $\psi(2S)$ mass. Uncertainties are statistical and systematic, respectively. The $N_i^{\rm comb}$ yields are calculable as $N_i^{\rm bkg} - N_i^{\rm peak}$.

	$\psi(2S) \to \nu\bar{\nu}$					
Channel	K^+	K^0	$K^{*+} \to K^+\pi^0$	$K^{*+} \to K_S^0\pi^+$	$K^{*0} \to K^+\pi^-$	$K^{*0} \to K_S^0\pi^0$
$N_i^{\rm peak}$	$1.4 \pm 0.4 \pm 0.1$	$0.6 \pm 0.3 \pm 0.1$	$1.4 \pm 0.4 \pm 0.1$	$1.0 \pm 0.3 \pm 0.1$	$3.5 \pm 0.7 \pm 0.3$	$0.6 \pm 0.2 \pm 0.1$
$N_i^{\rm bkg}$	$1.6 \pm 0.4 \pm 0.1$	$0.7 \pm 0.3 \pm 0.1$	$1.4 \pm 0.4 \pm 0.1$	$1.5 \pm 0.4 \pm 0.1$	$3.9 \pm 0.7 \pm 0.3$	$0.6 \pm 0.2 \pm 0.1$
$\varepsilon_i^{\rm sig}$ $(\times 10^{-8})$	$57.2 \pm 3.5 \pm 3.3$	$13.1 \pm 1.2 \pm 1.4$	$8.1 \pm 1.7 \pm 0.7$	$4.9 \pm 1.1 \pm 0.4$	$14.2 \pm 1.2 \pm 1.6$	$0.6 \pm 0.1 \pm 0.1$
$N_i^{\rm obs}$	3	1	1	3	5	1
$\mathcal{B}(\psi(2S) \to \nu\bar{\nu})$			$(5.6^{+7.4+1.6}_{-4.6-1.4}) \times 10^{-3}$			
Limit			$<15.5 \times 10^{-3}$			

limits are comparable with those obtained by BES for $J/\psi \to \nu\bar{\nu}$, in $\psi(2S) \to \pi^+\pi^- J/\psi$ [20].

VIII. SUMMARY

In conclusion, we have searched for the decays $B \to K\nu\bar{\nu}$ and $B \to K^*\nu\bar{\nu}$, as well as $J/\psi \to \nu\bar{\nu}$ and $\psi(2S) \to \nu\bar{\nu}$ via $B \to K^{(*)}J/\psi$ and $B \to K^{(*)}\psi(2S)$, recoiling from a hadronically reconstructed B meson within a data sample of 471×10^6 $B\bar{B}$ pairs. We observe no significant signal in any of the channels and obtain upper limits at the 90% CL of $\mathcal{B}(B \to K\nu\bar{\nu}) < 3.2 \times 10^{-5}$, $\mathcal{B}(B \to K^*\nu\bar{\nu}) < 7.9 \times 10^{-5}$, $\mathcal{B}(J/\psi \to \nu\bar{\nu}) < 3.9 \times 10^{-3}$, and $\mathcal{B}(\psi(2S) \to \nu\bar{\nu}) < 15.5 \times 10^{-3}$. The branching fraction central values and upper limits are consistent with SM predictions. We report $B \to K^{(*)}\nu\bar{\nu}$ branching fraction limits in Tables IV and V, and $c\bar{c} \to \nu\bar{\nu}$ branching fraction limits in Tables VI and VII. These results include the first lower limit in the $B^+ \to K^+\nu\bar{\nu}$ decay channel, the most stringent published upper limits using the hadronic-tag reconstruction technique in the $B^0 \to K^0\nu\bar{\nu}$, $B^+ \to K^{*+}\nu\bar{\nu}$, and $B^0 \to K^{*0}\nu\bar{\nu}$ channels, and the first upper limit for $\psi(2S) \to \nu\bar{\nu}$. We also present partial branching fraction values for $B \to K^{(*)}\nu\bar{\nu}$ over the full $s_B$spectrum in Fig. 6 in order to enable additional tests of new-physics models.

ACKNOWLEDGMENTS

We are grateful for the extraordinary contributions of our PEP-II colleagues in achieving the excellent luminosity and machine conditions that have made this work possible. The success of this project also relies critically on the expertise and dedication of the computing organizations that support *BABAR*. The collaborating institutions wish to thank SLAC for its support and the kind hospitality extended to them. This work is supported by the U.S. Department of Energy and National Science Foundation, the Natural Sciences and Engineering Research Council (Canada), the Commissariat à l'Energie Atomique and Institut National de Physique Nucléaire et de Physique des Particules (France), the Bundesministerium für Bildung und Forschung and Deutsche Forschungsgemeinschaft (Germany), the Istituto Nazionale di Fisica Nucleare (Italy), the Foundation for Fundamental Research on Matter (The Netherlands), the Research Council of Norway, the Ministry of Education and Science of the Russian Federation, Ministerio de Economía y Competitividad (Spain), and the Science and Technology Facilities Council (United Kingdom). Individuals have received support from the Marie-Curie IEF program (European Union) and the A. P. Sloan Foundation (USA).

[1] W. Altmannshofer, A. J. Buras, D. M. Straub, and M. Wick, J. High Energy Phys. 04 (2009) 022.
[2] L. N. Chang, O. Lebedev, and J. N. Ng, Phys. Lett. B **441**, 419 (1998).
[3] G. Buchalla, G. Hiller, and G. Isidori, Phys. Rev. D **63**, 014015 (2000).
[4] X.-Q. Li, Y.-D. Yang, and X.-B. Yuan, J. High Energy Phys. 03 (2012) 018.
[5] J. H. Jeon, C. S. Kim, J. Lee, and C. Yu, Phys. Lett. B **636**, 270 (2006).
[6] C. Bird, R. V. Kowalewski, and M. Pospelov, Mod. Phys. Lett. A **21**, 457 (2006).
[7] D. McKeen, Phys. Rev. D **79**, 114001 (2009).
[8] H. Davoudiasl, H.-S. Lee, and W. J. Marciano, Phys. Rev. D **85**, 115019 (2012).
[9] T. M. Aliev, A. S. Cornell, and N. Gaur, J. High Energy Phys. 07 (2007) 072.
[10] J. F. Kamenik and C. Smith, J. High Energy Phys. 03 (2012) 090.
[11] P. Colangelo, F. De Fazio, R. Ferrandes, and T. N. Pham, Phys. Rev. D **73**, 115006 (2006).
[12] B. McElrath, Phys. Rev. D **72**, 103508 (2005).
[13] P. Fayet, Phys. Rev. D **74**, 054034 (2006).
[14] The use of charge conjugate processes is implied throughout this article.
[15] P. del Amo Sanchez *et al.* (*BABAR* Collaboration), Phys. Rev. D **82**, 112002 (2010).

[16] B. Aubert *et al.* (*BABAR* Collaboration), Phys. Rev. D **78**, 072007 (2008).
[17] B. Aubert *et al.* (*BABAR* Collaboration), Phys. Rev. Lett. **94**, 101801 (2005).
[18] O. Lutz *et al.* (BELLE Collaboration), arXiv:1303.3719.
[19] K.-F. Chen *et al.* (BELLE Collaboration), Phys. Rev. Lett. **99**, 221802 (2007).
[20] M. Ablikim *et al.* (BES Collaboration), Phys. Rev. Lett. **100**, 192001 (2008).
[21] J. P. Lees *et al.* (*BABAR* Collaboration), arXiv:1301.2703 [Nucl. Instrum. Methods Phys. Res., Sect. A (to be published)].
[22] B. Aubert *et al.* (*BABAR* Collaboration), Nucl. Instrum. Methods Phys. Res., Sect. A **479**, 1 (2002).
[23] B. Aubert *et al.* (*BABAR* Collaboration), arXiv:1305.3560 [Nucl. Instrum. Methods Phys. Res., Sect. A (to be published)].
[24] S. Agostinelli *et al.* (Geant4 Collaboration), Nucl. Instrum. Methods Phys. Res., Sect. A **506**, 250 (2003).
[25] B. Aubert *et al.* (*BABAR* Collaboration), Phys. Rev. D **76**, 031102 (2007).
[26] J. P. Lees *et al.* (*BABAR* Collaboration), Phys. Rev. Lett. **109**, 101802 (2012).
[27] G. Punzi, eConf C030908, MODT002 (2003); arXiv:physics/0308063.
[28] E. Farhi, Phys. Rev. Lett. **39**, 1587 (1977).
[29] G. C. Fox and S. Wolfram, Phys. Rev. Lett. **41**, 1581 (1978).
[30] K. Nakamura *et al.* (Particle Data Group), J. Phys. G **37**, 075021 (2010), and 2011 partial update for the 2012 edition.
[31] M. Bartsch, M. Beylich, G. Buchalla, and D.-N. Gao, J. High Energy Phys. 11 (2009) 011.
[32] R. Barlow, Comput. Phys. Commun. **149**, 97 (2002).
[33] G. Buchalla, A. J. Buras, and M. E. Lautenbacher, Rev. Mod. Phys. **68**, 1125 (1996).